Angiostatin-Like Activity of a Monoclonal Antibody to the Catalytic Subunit of F_1F_0 ATP Synthase

Sulene L. Chi,[1] Miriam L. Wahl,[1] Yvonne M. Mowery,[1] Siqing Shan,[2] Somnath Mukhopadhyay,[3] Susana C. Hilderbrand,[3] Daniel J. Kenan,[1] Barbara D. Lipes,[1] Carrie E. Johnson,[1] Michael F. Marusich,[1,4,5] Roderick A. Capaldi,[1,4,5] Mark W. Dewhirst,[2] and Salvatore V. Pizzo[1]

Departments of [1]Pathology and [2]Radiation Oncology, Duke University Medical Center; [3]Program in Neuroscience, JL Chambers Biomedical Biotechnology Research Institute, North Carolina Central University, Durham, North Carolina; [4]Mitosciences LLC; and [5]Institute of Molecular Biology, University of Oregon, Eugene, Oregon

Abstract

The antiangiogenic protein angiostatin inhibits ATP synthase on the endothelial cell surface, blocking cellular proliferation. To examine the specificity of this interaction, we generated monoclonal antibodies (mAb) directed against ATP synthase. mAb directed against the β-catalytic subunit of ATP synthase (MAb3D5AB1) inhibits the activity of the F_1 domain of ATP synthase and recognizes the catalytic β-subunit of ATP synthase. We located the antibody recognition site of MAb3D5AB1 in domains containing the active site of the β-subunit. MAb3D5AB1 also binds to purified *Escherichia coli* F_1 with an affinity 25-fold higher than the affinity of angiostatin for this protein. MAb3D5AB1 inhibits the hydrolytic activity of F_1 ATP synthase at lower concentrations than angiostatin. Like angiostatin, MAb3D5AB1 inhibits ATP generation by ATP synthase on the endothelial cell surface in acidic conditions, the typical tumor microenvironment where cell surface ATP synthase exhibits greater activity. MAb3D5AB1 disrupts tube formation and decreases intracellular pH in endothelial cells exposed to low extracellular pH. Neither angiostatin nor MAb3D5AB1 showed an antiangiogenic effect in the corneal neovascularization assay; however, both were effective in the low-pH environment of the chicken chorioallantoic membrane assay. Thus, MAb3D5AB1 shows angiostatin-like properties superior to angiostatin and may be exploited in cancer chemotherapy. [Cancer Res 2007;67(10):4716–24]

Introduction

Tumor growth is dependent on new vascular growth (1–3), and angiostatin is a potent inhibitor of angiogenesis (4, 5). Angiostatin inhibits endothelial cell proliferation and migration, inducing apoptosis *in vitro* (4, 5). Angiostatin inhibits ATP synthase on the surface of endothelial and tumor cells (6–9). ATP synthase is a transmembrane enzyme found not only in the plasma membrane of bacteria and the inner mitochondrial membrane (10) but also on the surface of endothelial and tumor cells, where it synthesizes ATP (6, 11–13). The enzyme catalyzes ATP synthesis coupled to an electrochemical gradient and ATP hydrolysis-driven proton translocation. The enzyme complex is composed of a soluble F_1 formed from five subunits (α_3, β_3, γ, δ, and ε) and the membrane-bound F_0 forming the proton channel (Fig. 1*A*; ref. 14). On the cell surface, F_1 is oriented extracellularly, localizing ATP synthesis or hydrolysis to the external cell surface (6–8, 15). Transmembrane F_0 allows protons moving through the channel to be extruded from the cell. Three α- and β-subunits alternate in a hexagonal arrangement around a central cavity containing the γ-subunit. The α- and β-subunits are structurally similar, each formed from three domains. The apical NH_2-terminal domains interact to form a β barrel (Fig. 1*B* and *C*). The central domains contain the nucleotide-binding sites, which are catalytic in the β-subunit, but not the α-subunit (Fig. 1*C*). The third and COOH-terminal domains consist of α helices, which in the β-subunit interact with the rotating γ-subunit (14).

Inhibition of cell surface ATP synthase by angiostatin reduces cellular proliferation, and in combination with low extracellular pH (pH_e), intracellular acidification and cytotoxicity ensue (6–8, 16–18). Similar results were achieved with polyclonal antibodies targeting ATP synthase (6–8, 12). These studies suggest that angiostatin, or anti-ATP synthase antibodies, prevent intracellular pH (pH_i) regulation by cell surface ATP synthase under conditions of acidosis by inhibiting proton translocation across the membrane-embedded protein. The resultant intracellular acidosis renders the cells susceptible to cell death (9).

We have identified a monoclonal antibody (mAb) directed against the catalytic β-subunit of F_1 ATP synthase that binds and potently inhibits ATP synthase. The antibody recognition site lies in a region containing the active site of the β-subunit. At low pH_e, this antibody inhibits endothelial cell tube differentiation to a greater extent than angiostatin. Like angiostatin, this antibody causes deregulation of pH_i in endothelial cells at low pH_e, providing a potential mechanism for its effects on endothelial cells. *In vivo* studies show antiangiogenic activity of the antibody in the chorioallantoic membrane (CAM) assay, in which blood vessel growth occurs in an acidic environment similar to the tumor microenvironment. Conversely, the antibody does not inhibit angiogenesis in the normal physiologic pH environment of the rat corneal neovascularization assay.

Whereas angiostatin is relatively unstable with a serum half-life of 15 min (8), antibodies are stable with a typical half-life of ~20 days (8, 19). Humanized mAbs are well accepted as pharmaceutical agents with excellent yields and high affinity (16), raising the possibility of an angiostatin-mimetic mAb as a cancer therapeutic.

Materials and Methods

Materials. Recombinant *Escherichia coli* F_1 was cloned, expressed, and purified from plasmid pRA100 (20). Anti-ATP synthase (complex V) β-subunit mouse mAb directed against the β-catalytic subunit of ATP synthase (MAb3D5AB1), isotype IgGκ, was generated by murine immunization with

Requests for reprints: Salvatore V. Pizzo, Duke University Medical Center, Box 3712, Durham, NC 27710. Phone: 919-684-3529; Fax: 919-684-8689; E-mail: pizzo001@mc.duke.edu.

doi:10.1158/0008-5472.CAN-06-1094

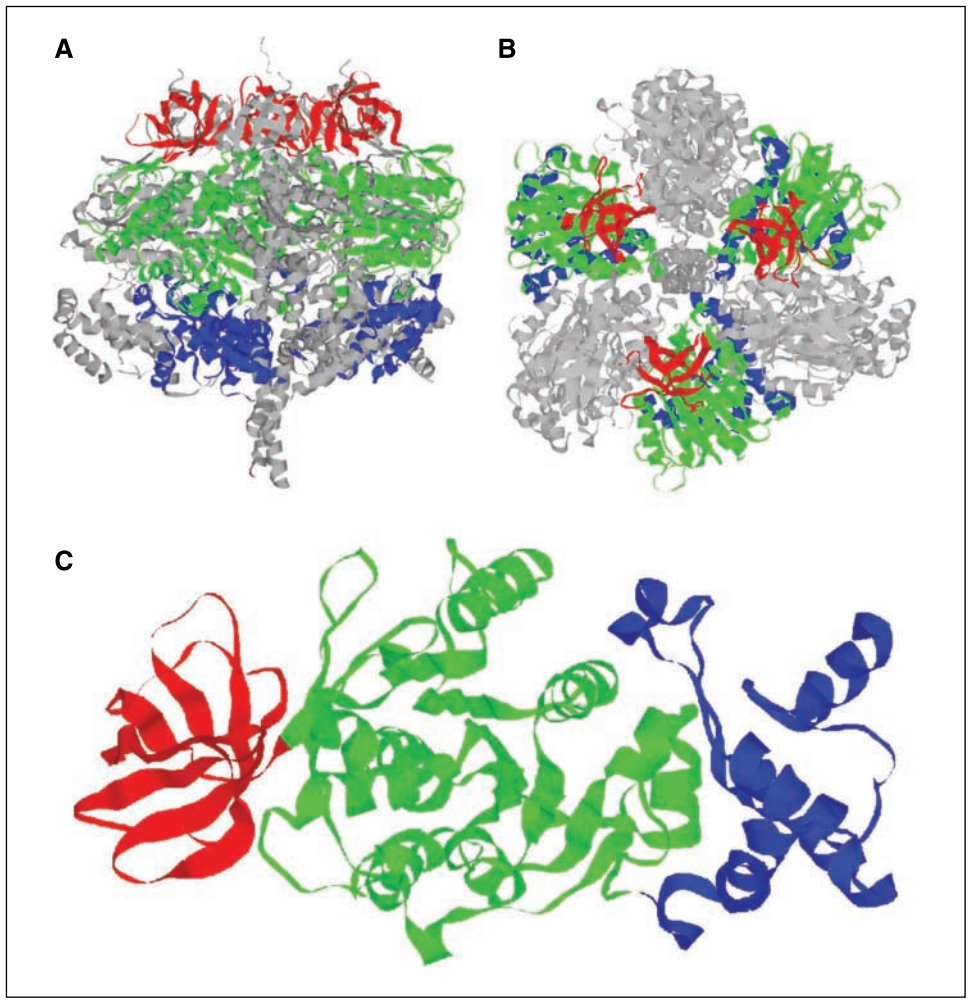

Figure 1. Relative position of the β-subunit within F_1 ATP synthase. The domains (*color*) of the catalytic β-subunit of human F_1 ATP synthase are represented in the context of the three-dimensional crystallographic structure of bovine F_1 ATP synthase (PDB ID: 1BMF; *gray scale*) in side profile (*A*) and from a bird's eye view looking downward at the alternating β barrels of the first domains of α- and β-subunits within F_1 ATP synthase (*B*). The domains of a β-subunit (*C*) in the ATP-bound conformation are identified individually within an isolated β-subunit; domain 1 (*red*), domain 2 (*green*), and domain 3 (*blue*). The breakpoints for the domains were chosen as follows: domain 1 forms a clearly delineated β barrel motif; domain 2 was separated from domain 3 by a flexible loop, with Met#408 chosen as the breakpoint between domains to facilitate soluble expression of individual domains 2 and 3. ATP synthesis and hydrolysis occur in domain 2, which contains the active nucleotide-binding site within the β-subunit. Domains 2 and 3 undergo conformational changes during enzymatic catalysis, with domain 3 interacting with the rotating γ-subunit extending the length of the F_1 component, whereas domain 1 remains relatively fixed in interactions with the β-barrel domains of adjacent α-subunits (*gray*) forming a hexameric tether of β barrels as seen in (*B*).

human heart mitochondria (21) with the following hybridoma partners: immune splenocytes derived from a murine F_1 hybrid of BALB/cJ and SLJ/J mice, and P3X63-AG8.653 myelomas. Screening was accomplished by Western blot, first to identify anti-complex V mAbs; second, sucrose gradient material to confirm anti-complex V mAbs; third, antigen identification by mass spectrometry; and fourth, immunocytochemical detection by the mAb of mitochondria in cultured fibroblasts. Recombinant human angiostatin was from Entremed. Fertilized chicken eggs were from Carolina Biological Supply. Fisher F344 female rats (8–10 weeks old, ~150 g) were from National Cancer Institute-Frederick. Recombinant human basic fibroblast growth factor (bFGF) was from R&D Systems. Sucrose octasulfate aluminum complex (sucralfate) and hydron polymer (poly2-hydroxylethylmethacrylate) were from Sigma.

Cells. Human umbilical vascular endothelial cells (HUVEC) were obtained from umbilical cords (22) under an Institutional Review Board–exempt protocol, as discard with no patient identifiers. HUVECs, passages 2 to 4, were grown in M199 with 20% FCS, 0.01% heparin (Sigma), 1.5% endothelial cell growth supplement (Collaborative Biochemicals), 1% penicillin-streptomycin, and 1% L-glutamine.

ELISA binding studies. Binding studies were done with purified, recombinant *E. coli* F_1 adsorbed onto Immulon 4× 96-well plates (Thermo Labsystems). Plates were coated with protein (0.75 μg/well) in 50 μL of 0.1 mol/L $NaHCO_3$ (pH 9.6) and incubated for 20 h at 4°C. Nonspecific sites were blocked by Superblock (Pierce) incubation for 1 h at room temperature. Increasing amounts of MAb3D5AB1 were added in a 50 μL final volume for 1 h at room temperature. Plates were washed and incubated with rat anti-mouse IgG1 biotin conjugate (1:4,500 dilution; Southern Biotech) for 1 h at room temperature. Plates were developed with TMB substrate (Sigma; ref. 6). Control studies were done in triplicate in the absence of ATP synthase to detect nonspecific binding. These values were averaged and subtracted from the averaged triplicate samples in the presence of ATP synthase. As a positive control, plates were coated with recombinant human β-subunit. Secondary rat anti-mouse antibody in the absence of primary antibody served as a further negative control for nonspecific binding.

Cell surface ATP generation assay. HUVEC P4 cells (70,000 per well) in 96-well plates were grown at 37°C, 5% CO_2 overnight. Cells were placed in serum-free medium and treated with MAb3D5AB1, piceatannol (Sigma), or medium alone for 30 min at 37°C, 5% CO_2 to achieve pH_e 7.2 or 17% CO_2 to achieve pH_e 6.7. Piceatannol, a known ATP synthase inhibitor, served as a positive control and to determine the component of cell surface ATP generation attributable to ATP synthase. Cells were incubated with ADP for 20 s, and supernatants were immediately removed and assayed for ATP production by CellTiterGlo luminescence assay (Promega; ref. 23).

Cloning of the β-subunit of ATP synthase and its domains. HUVEC mRNA was isolated and reverse transcribed using random primers into single-stranded cDNA. The β-subunit (Fig. 1) was PCR amplified using specific primers with an NH_2-terminal 6-His tag, as were domains 1, 2, and 3, domains 1 to 2, and domains 2 to 3 (Fig. 2*A*). To generate fusion proteins containing the NH_2-terminal 6-His tag with the domains of the β-subunit, primers were designed to introduce a *Nde*I restriction site at the 5′ end and an *Xho*I site at the 3′ COOH-terminal end (Table 1). Domain boundaries were determined based on structural motifs (Fig. 1*C*). Domain 1 included 50

amino acids of transit peptide at the NH_2 terminus to facilitate expression of recombinant proteins, as expression of the mature sequence was not possible. PCR products purified from 1.5% Tris-acetate/EDTA agarose gel using GFX PCR DNA and gel band purification kit (Amersham) were subcloned into pMOS*Blue* vector by blunt-end ligation using the pMOS*Blue* Blunt-End Cloning kit (Amersham). Competent *E. coli* DH5α (Life Technologies) were transformed with 1 μL ligation mixture/100 μL cells, plated on LB-ampicillin (100 μg/mL) and tetracycline (15 μg/mL) agarose plates, and grown overnight at 37°C. Colonies were screened for inserts with *Nde*I and *Xho*I (New England Biolabs) digestion followed by gel purification. The subcloned inserts were ligated into *Nde*I- and *Xho*I-digested pET24d vector (Novagen) using the Clonables kit (Novagen). Competent *E. coli* Novablue cells (Novagen) were transformed with ligation mixture and grown on LB-kanamycin agarose plates, and colonies were screened for insertion by restriction enzyme digestion and DNA sequencing.

Purification of the β-subunit of ATP synthase and its domains. Competent Rosetta(DE3)pLysS cells (Novagen) containing tRNAs recognizing rare codons were transformed with pET24d vector containing β-subunit or its domains, plated on LB-kanamycin and chloramphenicol agarose plates, and grown overnight at 37°C. Then, 2.5 mL LB, containing 30 μg/mL kanamycin and 34 μg/mL chloramphenicol, was inoculated with one colony and grown at 37°C, 200 rpm, to $A_{600\ nm}$ of 0.54, and stored overnight at 4°C. A 50 mL culture (LB, 30 μg/mL kanamycin, 34 μg/mL chloramphenicol) was inoculated with 2 mL of the noninduced overnight culture and grown at 37°C, 250 rpm, to $A_{600\ nm}$ of 0.60. Isopropyl thio-β-D-galactosidase was added to a final concentration of 1 mmol/L and cultures were grown an additional 2.5 h at 37°C, 250 rpm. Cells were harvested by centrifugation at 5,000 × *g* for 5 min and stored at −20°C. Lysates were prepared by denaturing with 8 mol/L urea for all proteins except β-domain 3, which was prepared under native conditions. Lysates were purified using Ni-NTA His

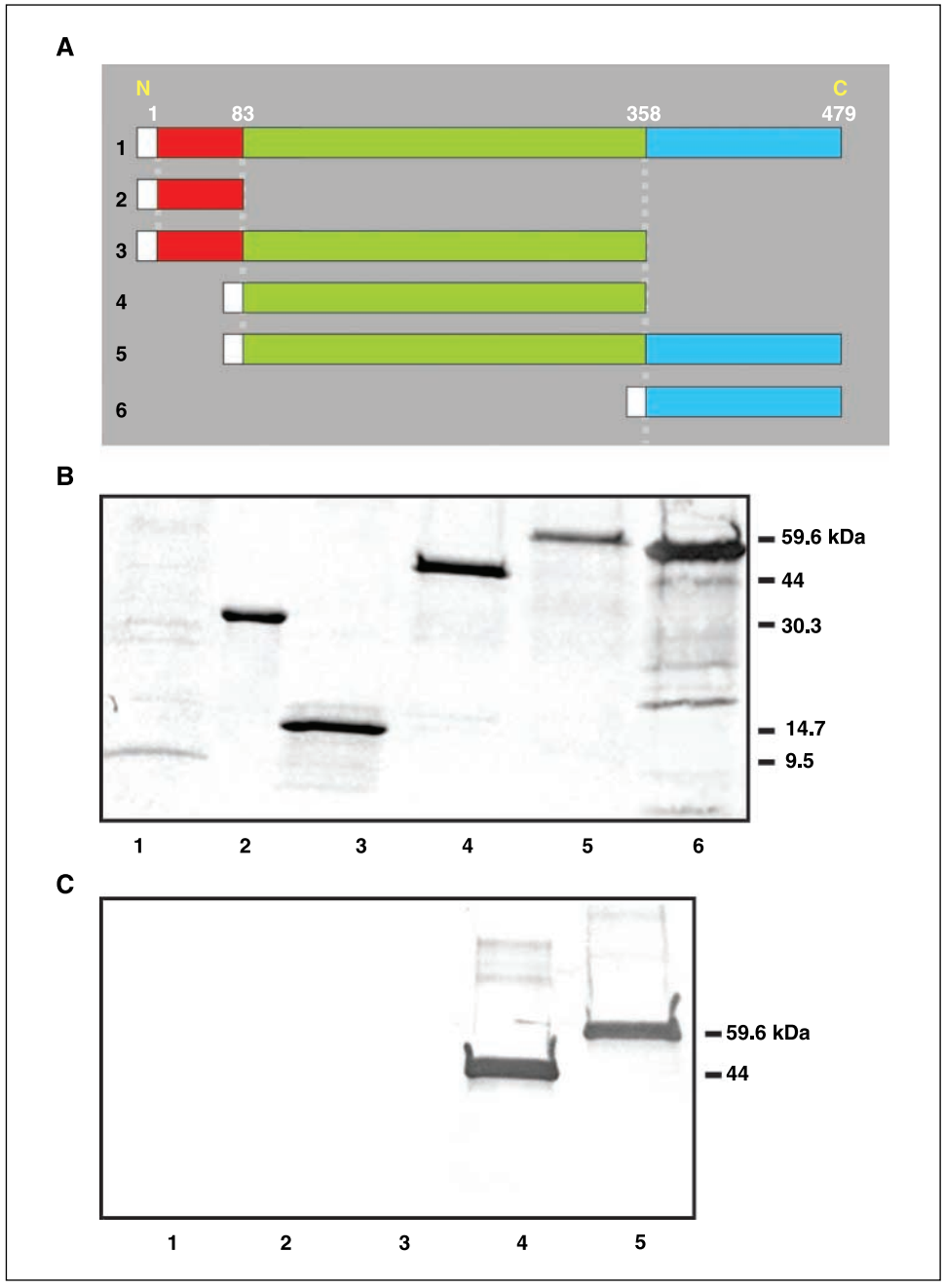

Figure 2. Expression and purification of fragments of the β-subunit of human F_1 ATP synthase. *A,* schematic diagram of relative location of domain constructs. A 6-His tag (*striped*) was cloned to the NH_2-terminal end of the human cDNA sequence for the β-subunit of F_1 ATP synthase (*1*). cDNA constructs of domain 1 (*2, red*), domains 1 and 2 (*3*), domain 2 (*4, green*), domains 2 and 3 (*5*), and domain 3 (*6, blue*) with 6-His tags and amino acids of domain breakpoints labeled. Residue numbers are based on human F_1 ATP synthase structure ATPB_human, SWISS-PROT accession no. P06576. *B,* purification of six 6-His-tagged recombinant domains of human F_1 ATP synthase β-subunit. Purified proteins were analyzed by SDS-PAGE on a 10% to 20% Tris-HCl gel, transferred to PVDF, and stained with Coomassie brilliant blue. β-subunit: domain 1 (*lane 1*), domain 2 (*lane 2*), domain 3 (*lane 3*), domains 2 and 3 (*lane 4*), domains 1, 2, and 3 (entire α-subunit; *lane 5*), and domains 1, 2, and 3 (entire α-subunit; *lane 6*). Molecular weights of the constructs. This transfer was identical to the PVDF used in (*C*) to determine the antigen recognition site of MAb3D5AB1 and served as a negative control to insure all constructs transferred to PVDF. *C,* immunoreactivity of MAb3D5AB1 to F_1 ATP synthase β-subunit. Purified, recombinant domains of β-subunit of human F_1 ATP synthase submitted to SDS-PAGE and Western blotting were detected by MAb3D5AB1. Immunoblotting with MAb3D5AB1 revealed no detection of the constructs of individual domain 1 (*lane 1*), domain 2 (*lane 2*), or domain 3 (*lane 3*) of the α-subunit but robust detection of domains 2 and 3 (*lane 4*) and the entire β-subunit (*lane 5*). A control blot with secondary antibody alone was negative, indicating the absence of any nonspecific binding (data not shown).

Table 1. Primer sequences used for construction of 6-His-tagged domains of the β-subunit of human F_1 ATP synthase

Domain	5′ Primer sequence	3′ Primer sequence
1	CTTGGT**CATATG**CAC	CGGTGA**CTCG**
	CACCACCACCACC	**AG**TTA*GATT*
	AC*ACATCTCCTTC*	*GGTGCACCAG*
	GCCAAAAGC	*AATCCAGTAC*
2	CTTCGT**CATATG**CACCA	CGGTGA**CTCGA**
	CCACCACCACCAC*AA*	**G**TTA*GATAC*
	AATTCCTGTTGGTCCT	*GAGAGGTGG*
	GAGACTTTGGGC	*AGTCTAGAG*
3	CTTCGT**CATATG**CAC	CGGTGA**CTC**
	CACCACCACCACC	**GAG***tcacgat*
	AC*ATGGATCCCAA*	*gaatgctctt*
	CATTGTTGGCAG	*cagcca*

NOTE: Sequences are based on the cDNA of human F_1 ATP synthase (protein accession no. X03559, *italics*). Restriction enzyme sites, in bold, represent for 5′ end primers, an *Nde*I cleavage site, and for 3′ primers, an *Xho*I site. Primers read from 5′ to 3′ with respect to cDNA. For constructs spanning two domains, the appropriate combinations of primers were used. For example, for domains 2 and 3, the 5′ primer for domain 2 was used in conjunction with the 3′ primer for domain 3.

Bind Resin columns (Novagen) and the resulting proteins were dialyzed against PBS (pH 7.0).

Western blotting. Purified, recombinant β-domain proteins (~1 μg) under reducing conditions were separated by SDS-PAGE and transferred to polyvinylidene difluoride (PVDF; Roche). Membranes were blocked overnight at 4°C, incubated with MAb3D5AB1 at 2.5 mg/mL for 2 h at room temperature, and washed. Membranes were incubated with antimouse alkaline phosphatase conjugate (Sigma), washed, and developed with 5-bromo-4-chloroindol-3-yl-phosphate nitroblue tetrazolium. To insure that the secondary detection antibody did not contribute to background detection, a membrane was developed with secondary antibody alone. To confirm transfer of all protein domains to the membrane, a post-transfer membrane was stained with Coomassie brilliant blue.

ATP synthase F_1 activity assay. Fresh bovine heart mitochondria were sonicated to yield submitochondrial particles. F_1 was separated from membrane-bound F_0 by chloroform extraction and purified (6). Purified F_1 exhibits ATP hydrolytic activity alone, as ATP synthesis requires association with F_0 to couple the proton gradient across F_0 with the rotational motion of F_1. Therefore, we measured F_1 ATP hydrolytic activity by coupling ADP generation to NADH oxidation via pyruvate kinase and lactate dehydrogenase reactions (24).

Fluorescence microscopy. HUVECs were plated in Matrigel-coated (BD Biosciences) eight-well slides at a density of 70% confluency. Cells were washed, fixed under nonpermeabilized conditions, and blocked (17). Cells were incubated with a mAb to ATP synthase (1:50 in DPBS) for 1 h/37°C. Cells were washed, incubated with a Cy3 secondary antibody, and visualized along with identification of endothelial cell nuclei as described (17). For each treatment, 10 fields of cells were examined.

HUVEC tube formation on Matrigel. Plates (Collaborative Biomedicals) were coated with Matrigel at 4°C (300 μL/well at 15 mg/mL) and incubated at 37°C/30 min. HUVECs (50,000 per well) were plated and incubated for 6 h in the presence or absence of MAb3D5AB1 (10–100 μg/mL) in normal- or low-pH medium at 37°C, 5% CO_2 to allow tube formation. Cells were fixed, stained, and quantified in triplicate (17, 18).

pH_i measurements. pH_i was measured by fluorescence in HUVEC (17, 18). Cells were incubated for 15 min with 9 μmol/L carboxy snarf-1 acetoxymethyl ester (Molecular Probes) in medium containing 10% fetal bovine serum at 37°C, 5% CO_2 (25, 26). After steady-state readings were established in medium (pH 7.4), it was removed, and 1 mL medium (pH 6.7) with or without MAb3D5Ab1 (10 μg/mL final concentration) was introduced. Experiments were repeated at least twice, with three to five measurements per field. pH_i was obtained from the whole emission spectra emitted by the cells and collected on an inverted microscope (Nikon Diaphot, Nikon, Inc.; refs. 17, 18). Calibration procedures are as described (27); however, 140 wavelengths (whole fluorescence spectra) were used to calculate pH_i (17, 18, 25, 28).

pH_e measurements. pH_e measurements in the CAM assay were made using a Sentron ISFET pH meter, designed for use with solids and viscous materials. Corneal micropocket pH measurements were made with a Fisher accumet pH meter equipped with a 21-gauge protected needle microelectrode for pH and a flexible microreference electrode from Microelectrodes, Inc.

Rat corneal neovascularization assay. Animal experiments were done as approved by the Duke University Institutional Animal Care and Use Committee. The rat corneal neovascularization assay was done as described (29). Sustained-release pellets contained equal volumes of Hydron (12% w/v in ethanol) and a solution of bFGF (100 ng), sucralfate (100 μg), and drug or PBS (negative control). MAb3D5AB1 was used at 650 ng/pellet and angiostatin at 20 μg/pellet. Vascular area density and average vessel length were measured by an investigator blind to treatment assignment using ImageJ software (29).

Chicken CAM assay. The CAM assay was done as described (30). Test compounds (bFGF, angiostatin ± bFGF, MAb3D5AB1 ± bFGF, or PBS) were dried onto a sterile quarter of a 13-mm Thermanox disc (Nunc) and placed onto the CAM on day 10. After 70 ± 4 h, CAMs were photographed and analyzed by an investigator blind to treatment assignment.

Results

MAb3D5AB1 binding studies. We have identified ATP synthase on the endothelial cell surface (6, 7). We now show that MAb3D5AB1 targeting the human β-subunit also recognizes ATP synthase on nonpermeabilized HUVEC as visualized by fluorescence microscopy (Fig. 3*A* and *B*). MAb3D5AB1 binds to purified, recombinant *E. coli* F_1 in a concentration-dependent and saturable manner (Fig. 3*C*). Human and *E. coli* ATP synthase exhibit 70% homology in the α-subunit (SWISS-PROT accession nos. P25705 and P00822, respectively) and 80% homology in the β-subunit (P06576 and P00824). Background binding of MAb3D5AB1 to BSA-coated wells was comparable with the baseline, indicating that MAb3D5AB1 binds specifically to F_1. Apparent dissociation constants [$K_{d(app)}$] were determined from double-reciprocal Scatchard plots of the binding data (Fig. 3*C, inset*). The $K_{d(app)}$ for MAb3D5AB1 binding to purified *E. coli* F_1 is 16 nmol/L compared with 405 nmol/L for angiostatin binding to *E. coli* F_1 (6). Thus, MAb3D5AB1 targets the angiostatin receptor ATP synthase with a binding affinity 25-fold greater than angiostatin.

Mapping of the MAb3D5AB1 antibody recognition site. For epitope mapping, a series of expression constructs of human F_1 domains were generated. These included the α-subunit, β-subunit, individual domains 1, 2, and 3 of the β-subunit, and a construct comprising domains 2 and 3 (Fig. 2*B*). The construct spanning domains 1 and 2 could not be expressed. By Western blot assays, MAb3D5AB1 strongly detected the β-subunit domains 2 and 3 and full-length recombinant β-subunit (Fig. 2*C*). MAb3D5AB1 did not recognize either the individual second or third domains of the β-subunit (Fig. 2*C*) nor the α-subunit of F_1, included as a negative control (data not shown). The remainder of the mAbs assessed recognized the α-subunit but not the β-subunit of F_1 (data not shown). These results show that MAb3D5AB1 targets the catalytic

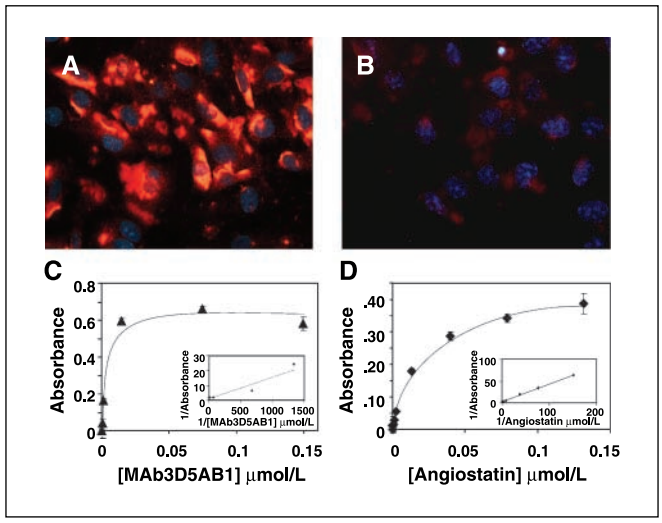

Figure 3. Binding studies of MAb3D5AB1 to HUVEC or to purified *E. coli* F_1 ATP synthase. *A,* MAb3D5AB1 detects F_1F_0 ATP synthase on HUVEC. F_1F_0 ATP synthase on nonpermeabilized HUVEC was detected by immunostaining with MAb3D5AB1 to the β-subunit of F_1F_0 ATP synthase and visualization with fluorescence microscopy. *B,* HUVEC immunostained with antimouse Cy3-conjugated secondary antibody alone as a negative control. Representative images ($n = 10$). *C* and *D,* an ELISA was done to determine concentration-dependent binding of mAb MAb3D5AB1 (*C*), or angiostatin (*D*), to a constant amount of F_1 ATP synthase. Each well was coated with 0.75 μg recombinant *E. coli* F_1 ATP synthase before addition of increasing amounts of antibody or angiostatin. Average background binding of secondary antibody alone from controls in triplicate was subtracted from the average absorbance in triplicate with MAb3D5AB1 or angiostatin. *Insets,* apparent dissociation constants [$K_{d(app)}$] were determined from double-reciprocal Scatchard plots of the binding data.

β-subunit of ATP synthase and binds within the region of the two domains involved in subunit activity.

MAb3D5AB1 inhibits purified bovine F_1 ATP synthase activity. ATP synthase holoenzyme catalyzes both the forward ATP synthesis and the reverse ATP hydrolysis reactions. Purified F_1 is restricted to catalyzing ATP hydrolysis. The ATP hydrolytic activity of purified bovine F_1 was measured by an enzymatic assay, in which a decrease in $A_{340\ nm}$ indicates ATP hydrolysis (24). MAb3D5AB1 inhibited purified ATP hydrolysis in a dose-dependent manner with maximal inhibition of ~60% at the highest antibody concentration assessed (40 μg/mL, ~0.27 μmol/L; Fig. 4*A*). None of the mAbs recognizing the α-subunit affected enzymatic activity of F_1 ATP synthase (data not shown). Angiostatin at a much higher concentration (10 μmol/L) achieves comparable inhibition (6). Neither mouse IgG, DPBS, nor assay buffer affected activity. Angiostatin exhibits enhanced activity on endothelial cells at pH_e 6.7 (8, 17, 18). Therefore, we examined the effect of low pH_e on the ability of MAb3D5AB1 to inhibit ATP synthase. There was no difference in the inhibitory activity of MAb3D5AB1 on purified ATPase activity at pH_e 6.8 compared with pH_e 7.2. Thus, mAb MAb3D5AB1 to the β-subunit inhibits ATP synthase activity with greater potency than angiostatin.

MAb3D5AB1 inhibits ATP generation on the cell surface of HUVEC at low pH_e. MAb3D5AB1 inhibits, in a dose-dependent manner, ATP generation by ATP synthase on HUVEC exposed to low pH_e compared with HUVEC at physiologic pH_e (Fig. 4*B*). This pH dependency agrees with previous findings that angiostatin and a polyclonal antibody to ATP synthase inhibited tumor cell surface ATP synthase to a greater degree under conditions of acidosis (6, 12). At low pH_e and comparable concentration, MAB3D5AB1 inhibited ATP synthesis at the endothelial cell surface to a greater extent than polyclonal antibody to ATP synthase or angiostatin (12). These results show that MAb3D5AB1 inhibits the activity of endothelial cell surface ATP synthase on intact cells with selective potency at low pH_e.

MAb3D5AB1AB1 affects pH_i at low pH_e. To determine whether MAb3D5AB1, like angiostatin (8, 12, 17, 18), interferes with pH_i regulation during acute extracellular acidification, HUVECs were challenged with a pH_e decrease from 7.3 to 6.7 in the presence or absence of MAb3D5AB1 (10 μg/mL; ~67 nmol/L; Fig. 4*C*), consistent with the concentration used in the tube formation assay. As a negative control, cells were exposed to extracellular acidification without antibody. Extracellular acidification resulted in pH_i decrease from 7.17 ± 0.03 to 6.92 ± 0.01, a net pH_i decrease of 0.25. In cells subjected to extracellular acidification with MAb3D5AB1, pH_i decreased to a greater extent, from 7.27 ± 0.004 to 6.86 ± 0.004, indicating a net change in pH_i of 0.41. Thus, the change in pH_i due to MAb3D5AB1 alone was 0.16. In comparison, a pH_i decrease of a comparable amount (0.45) to that observed from MAb3D5AB1 (10 μg/mL; ~67 nmol/L), requires a much higher concentration of angiostatin (30 μg/mL; ~1 μmol/L; ref. 18). MAb3D5AB1 therefore affects the pH_i of endothelial cells in a manner similar to angiostatin, but to a greater extent.

MAb3D5AB1 inhibits HUVEC tube formation at low pH_e. Angiostatin disrupts endothelial cell tube formation at low pH_e (18); therefore, we examined whether MAb3D5AB1 would act similarly. Endothelial cell tube formation was inhibited by 10 μg/mL (~67 nmol/L) MAb3D5AB1 at pH_e 6.7, whereas the antibody had no effect at pH_e 7.4 (Fig. 5*A*). At pH_e 6.7, tube formation was inhibited by ~60% in the presence of 10 μg/mL MAb3D5AB1 compared with cells treated with MAb3D5AB1 at pH_e 7.4 (Fig. 5*B*). Six other mAbs generated to F_1 recognizing the α-subunit did not significantly inhibit tube formation at low pH_e compared with the control of low pH_e alone (Fig. 5*B*). Previously, we showed that angiostatin at 10 μg/mL (~320 nmol/L) inhibited tube formation at pH_e 6.7 by ~33% (18). MAb3D5AB1 induces a greater inhibitory effect on endothelial cell tube formation than angiostatin at low pH_e.

MAb3D5AB1AB1 inhibits the development of neovasculature in the CAM assay but not the rat corneal neovascularization assay. To examine the antiangiogenic effect of MAb3D5AB1 *in vivo*, the antibody was tested in the chicken CAM assay and the rat corneal micropocket assay. In the CAM assay, blood vessel growth was stimulated with bFGF, and the effect of applying MAb3D5AB1 or angiostatin to the CAM was observed (Fig. 6*A–C*). Treatment with either of these compounds inhibited angiogenesis, as evidenced by decreased vessel ingrowth and branching visible on the treated area of these CAMs. At an ~18-fold lower molar dose, MAb3D5AB1 showed an equivalent antiangiogenic effect relative to angiostatin (Fig. 6*D*). Negative controls included eggs treated with PBS, MAb3D5AB1, or angiostatin without bFGF. These treatments had neither an angiogenic nor an antiangiogenic effect on the CAM (data not shown). Thus, neither angiostatin nor the antibody inhibited normal vessel development that occurs in the CAM, but both inhibited bFGF-dependent neovascularization. These findings are consistent with results of the human clinical trial of angiostatin, in which normal vasculature was not affected by exogenously administered angiostatin (31).

In the rat corneal micropocket assay, bFGF-stimulated corneal neovascularization was not inhibited by treatment with MAb3-D5AB1 or angiostatin. Average vessel length actually showed a trend

toward increased length in corneas treated with bFGF+MAb3D5AB1 (P = 0.09) or bFGF+angiostatin (P = 0.12) relative to bFGF alone, but the difference was not statistically significant. There was also no statistically significant difference between the vascular area density of bFGF-treated corneas versus corneas treated with bFGF+angiostatin (P = 0.66). The vascular area density was significantly higher in corneas treated with bFGF+MAb3D5AB1 than in corneas treated with bFGF alone (P = 0.04).

Because the effects of angiostatin and the antibody are pH dependent, we hypothesized that the pH of the rat cornea may be too high to achieve a significant antiangiogenic effect with these drugs. We used a pH microelectrode to determine the pH inside the corneal pocket before implanting the Hydron pellet. The corneal pH measured 7.47 $\pm$ 0.17 (n = 5), which is well above the optimal pH range for angiostatin and MAb3D5AB1. We repeated these pH measurements 6 days after implantation of the pellet containing bFGF with or without MAb3D5AB1. The average pH was 7.38 $\pm$ 0.14, with four of the five corneal pHs decreasing slightly. Despite this decrease in corneal pH after treatment with bFGF and MAb3D5AB1, the pH remained above the range required for MAb3D5AB1 to be active. Given that MAb3D5AB1 and angiostatin inhibited bFGF-induced neovascularization in the CAM assay, we also measured the pH of fertilized egg yolks and albumin. We found that the pH of the egg yolk is 5.89 $\pm$ 0.15. The pH of albumin is considerably higher (9.05 $\pm$ 0.06); however, the albumin is withdrawn from the eggs 5 days before treatment of the CAM. We hypothesized that the low pH present in the fertilized chicken CAM compared with the rat cornea accounts for the difference in the results of these two assays. Moreover, these *in vivo* studies are in accord with our *in vitro* data described above.

Discussion

Angiostatin binds to, and inhibits, ATP synthase on the endothelial cell surface, resulting in the reduction of cell proliferation (6, 7). Angiostatin also disrupts endothelial cell tube formation and pH_i regulation under conditions of acidosis (17, 18). Here, we show that the mAb MAb3D5AB1 (*a*) binds to the catalytic β-subunit of ATP synthase, (*b*) recognizes an epitope within the domains of the β-subunit involved in enzymatic activity, (*c*) binds F_1 specifically with high affinity compared with angiostatin, (*d*) inhibits the enzymatic activity of F_1 ATP synthase, (*e*) inhibits tube formation by endothelial cells at low pH, (*f*) affects pH_i of endothelial cells at low pH_e, and (*g*) inhibits angiogenesis in the CAM assay, in which pH_e is low.

Following immunization of mice with purified *E. coli* F_1 ATP synthase, we purified 21 murine mAbs. Of these, only one antibody

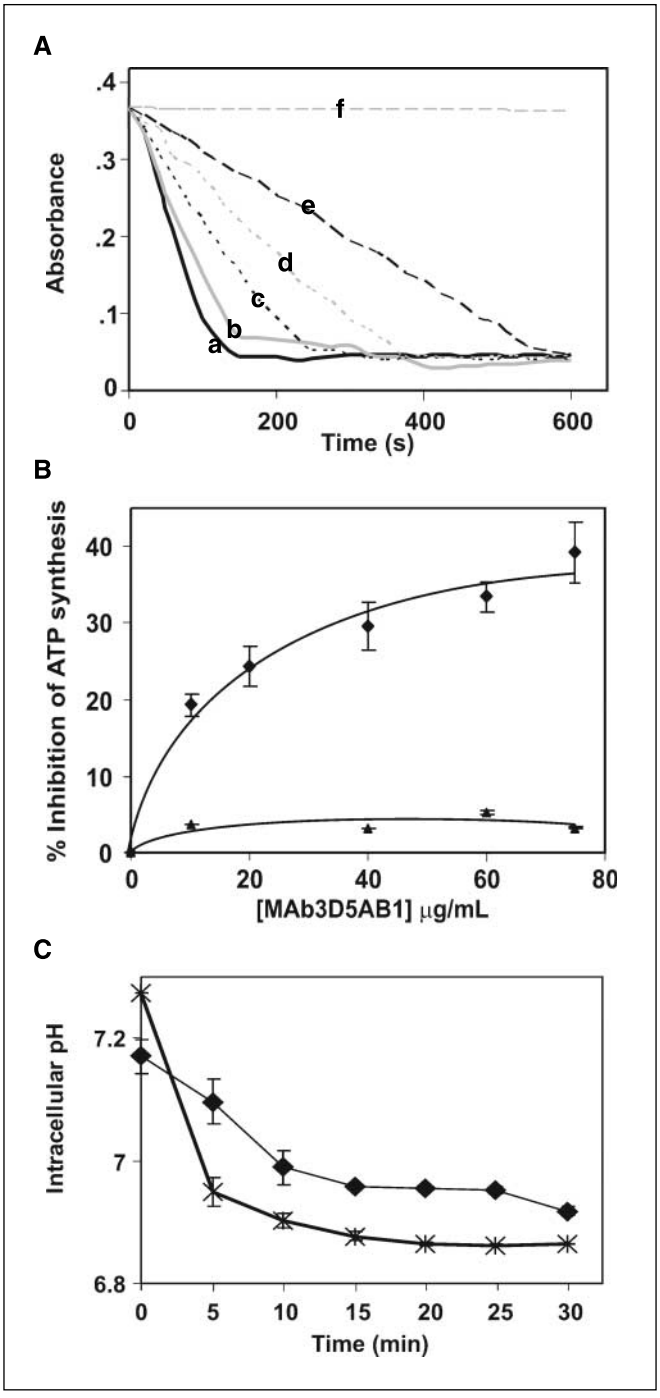

Figure 4. MAb3D5AB1 inhibits ATP synthase activity and affects pH_i of HUVEC. *A,* inhibition of purified F_1 ATP synthase by MAb3D5AB1. Purified F_1 ATP synthase activity was measured spectrophotometrically at λ of 340 nm by coupling the production of ADP to the oxidation of NADH via the pyruvate kinase and lactate dehydrogenase reaction, in which a decrease in the absorbance at λ of 340 nm indicates ATP hydrolysis and thus active protein. MAb3D5AB1 inhibited purified F_1 ATP synthase in a dose-dependent manner at 0 μg/mL (*a*), 5 μg/mL (*b*), 10 μg/mL (*c*), 20 μg/mL (*d*), and 40 μg/mL (*e*). Sodium azide (NaN_3, 2%), a known F_1 ATP synthase inhibitor, was used as a positive control to show 100% inhibition (*f*). Representative data (n = 3). *B,* inhibition of cell surface ATP generation by MAb3D5AB1 at low pH_e. Extracellular ATP generation on HUVEC was measured by bioluminescent surface assay following 20-s incubation with medium in the presence or absence of ADP. MAb3D5AB1 inhibits piceatannol-sensitive ATP synthesis on the cell surface of HUVEC at low pH_e (6.7) compared with neutral pH_e (7.2). Piceatannol is a stilbene phytochemical that inhibits F_1F_0 ATP synthase. *Points,* the percentage decrease in piceatannol-sensitive ATP synthesis in cells treated with MAb3D5Ab1 was calculated by dividing the average luminescent intensity for cells at a given pH treated with a single concentration of MAb3D5AB1 by the average luminescent intensity for untreated cells at the same pH (n = 4); *bars,* SD. *C,* pH_i in HUVEC was monitored as a function of time at 5-min intervals over 30 min following an acute intracellular acidification of pH_e from 7.4 to 6.7. First, at pH_e 7.4, five initial steady-state readings of pH_i established that the cells were at steady state. Next, acute extracellular acidification was introduced by replacement of the original 1 mL medium with 1 mL low pH_e 6.7 medium containing 0 (♦) or 10 μg/mL MAb3D5AB1 (X). MAb3D5AB1 treatment caused intracellular acidification compared with pH_e 6.7 medium alone. Three pH_i readings per coverslip plate were taken every 5 min for a 30-min time course beginning at the time of extracellular acidification and averaged. Each experiment was repeated two or three times. *Points,* average pH_i for the two treatment groups; *bars,* SD.

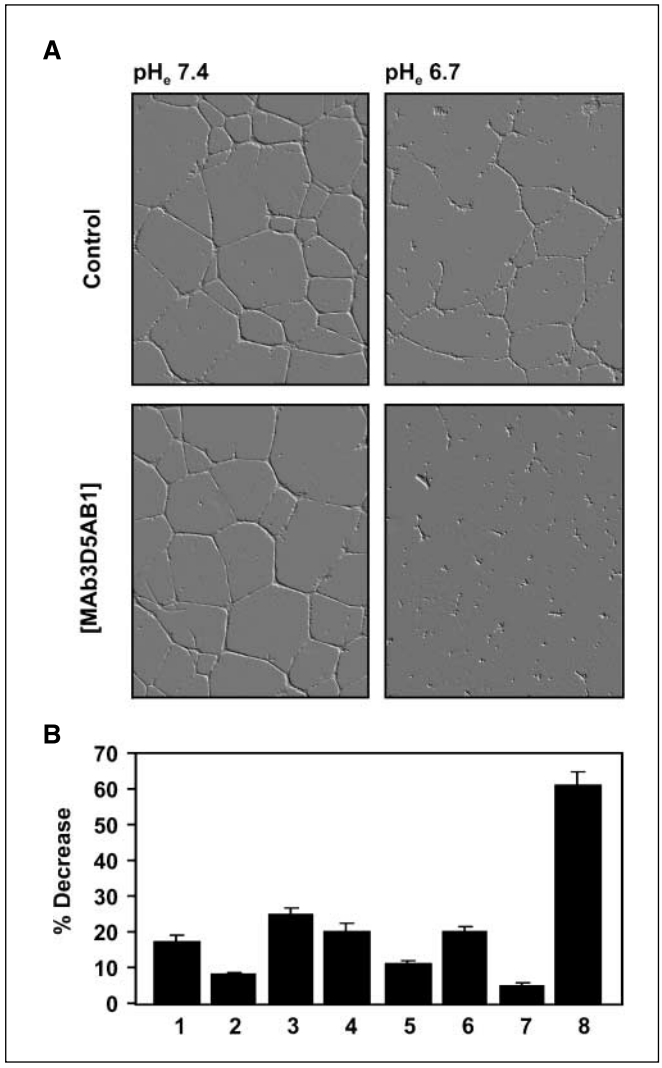

Figure 5. MAb3D5AB1 inhibits endothelial cell tube formation at low pH$_e$. *A,* HUVECs were plated on Matrigel at pH$_e$ 7.4 or 6.7, with either 0 or 10 μg/mL MAb3D5AB1. Representative fields. In the presence of 10 μg/mL MAb3D5AB1, tube formation is significantly disrupted at pH$_e$ 6.7 compared with cells at pH$_e$ 7.4 and to cells at pH$_e$ 6.7 in the absence of MAb3D5AB1. *B,* HUVECs were plated on Matrigel at pH$_e$ 7.4 or 6.7, with either 0 or 10 μg/mL of each of six mAbs to human F_1 ATP synthase. For each treatment group, 10 representative 1-mm^2 regions were quantified per data point at a ×15 magnification and averaged. The percentage decrease in average tube area was reported for pH$_e$ 6.7 compared with pH$_e$ 7.4. Compared with a control of no antibody, six mAbs to the α-subunit of F_1 ATP synthase did not inhibit tube formation significantly (*columns 2–7*), whereas MAb3D5AB1 inhibited tube formation by 60% (*column 8*).

recognized the catalytic β-subunit of F_1 ATP synthase and inhibited F_1 ATP synthase activity. The remaining mAbs recognized the noncatalytic α-subunit of F_1. ELISA binding assays established that the anti-β-subunit mAb, MAb3D5AB1, bound to bovine and *E. coli* F_1, and to the latter with a $K_{d(app)}$ of 16 nmol/L. Comparatively, angiostatin binding to *E. coli* F_1 ATP synthase showed a $K_{d(app)}$ of 405 nmol/L, establishing a higher binding affinity of MAb3D5AB1 for F_1 ATP synthase.

To determine the region of the epitope recognized by MAb3D5AB1, we generated recombinant domains of the human F_1 β-subunit. MAb3D5AB1 binds preferentially to the construct spanning domains 2 and 3, although not to separate constructs of domain 2 or 3. MAb3D5AB1 recognition of the protein encompassing domains 2 and 3, but not the individual domains, may localize the epitope to a junctional sequence spanning the domains. Because domains 2 and 3 are crucially involved in the enzymatic activity of F_1 ATP synthase–domain 2 contains the active nucleotide binding pocket, and the motion of enzyme catalysis is transduced through domains 2 and 3 (32–35)–it is not surprising that an antibody binding this region should exhibit inhibitory effects on F_1 ATP synthase activity.

Indeed, in an *in vitro* assay measuring F_1 hydrolytic activity, the only anti-F_1 monoclonal showing enzymatic inhibition was MAb3D5AB1, which recognizes the highly conserved and catalytic β-subunit. Furthermore, MAb3D5AB1 inhibition of F_1 was dose dependent and, at a concentration of 40 μg/mL (~0.27 μmol/L), achieved similar inhibition of ATP synthase activity as angiostatin at a much higher concentration of 10 μmol/L (6). The clinical importance of the β-subunit of ATP synthase in cancer remains to be elucidated, but studies have shown down-regulation of the β-subunit in several human cancers (34). Apparently, down-regulation of the angiostatin receptor protects these cancerous cells from the effects of locally circulating angiostatin.

Proton translocation across F_0 is coupled to the rotation of F_1. Thus, we expected that as MAb3D5AB1 inhibited both bidirectional ATP synthase enzymatic actions of ATP synthesis and hydrolysis, proton translocation across the endothelial cell membrane by F_1F_0 ATP synthase might also be impaired by MAb3D5AB1. Angiostatin and polyclonal antibodies against ATP

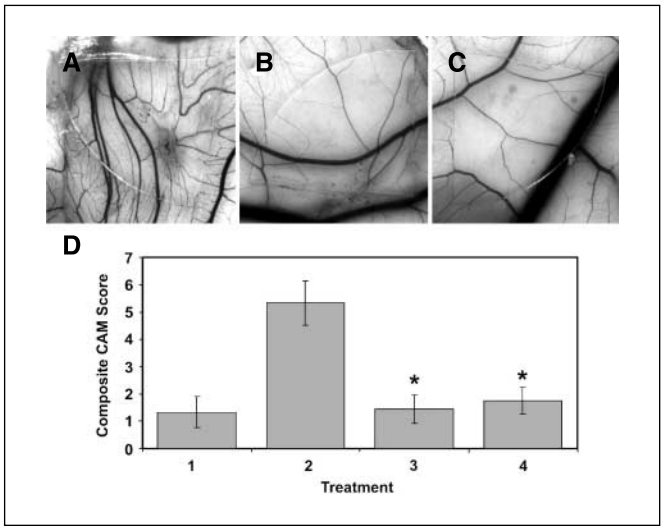

Figure 6. MAb3D5AB1 and angiostatin inhibit bFGF-stimulated angiogenesis in the chicken CAM model. *A* to *C,* representative images of CAMs treated with bFGF alone (*A*), bFGF+MAb3D5AB1 (*B*), and bFGF+angiostatin (*C*). Treatment with MAb3D5AB1 (8 μg) or angiostatin (30 μg) inhibited bFGF-stimulated angiogenesis. *D,* inhibition of angiogenesis in the CAM model by MAb3D5AB1 and angiostatin. All CAMs were assigned a score on a scale of 1 to 6 by an investigator blind to the treatment assignment of CAM. This score was based on assessment of vascular ingrowth, branching, and density in the CAM area treated under the Thermanox disc. A score of 1 was assigned to CAMs that showed no increased vascularization above the normal level in the CAM model. A score of 6 was assigned to CAMs showing the maximum degree of vascularity obtained in these assays. *Columns,* mean score; *bars,* SD. A two-sample unpaired *t* test with unpooled variance was used for statistical analysis in the *in vivo* studies. Treatment with PBS (*1*) resulted in no increased vascularization compared with an untreated CAM. CAMs treated with bFGF+MAb3D5AB1 (*3*) or bFGF+angiostatin (*4*) showed a statistically significant decrease in angiogenesis relative to CAMs treated with bFGF alone (*2*). *, $P < 0.001$.

synthase inhibit F_1 ATP synthase activity and affect proton translocation across the cell membrane, causing intracellular acidosis (8, 12, 15). Here, we showed that MAb3D5AB1 markedly inhibited cell surface ATP generation only at low pH_e, suggesting that MAb3D5AB1 would have a greater effect on HUVEC pH_i regulation by cell surface ATP synthase at low pH_e. Indeed, we observed that MAb3D5AB1 treatment depressed pH_i of endothelial cells under conditions of external acidosis. The observed intracellular acidification was achieved by a molar concentration of antibody over 10-fold less than of angiostatin, as determined in a previous study (18). These results strongly suggest that, as with angiostatin, MAb3D5AB1, which binds specifically to ATP synthase, inhibits the enzymatic and proton-pumping actions of ATP synthase, resulting in compromised enzymatic activity and pH_i. Acidosis is a characteristic common to the tumor microenvironment, resulting from inefficient tumor vasculature and tumor reliance on glycolytic metabolism with attendant generation of lactic acid. The apparent efficacy of MAb3D5AB1 under conditions of low pH_e may be due to increased activity of cell surface ATP synthase (12) and, hence, greater effect of inhibition of the ATP synthase.

With evidence that MAb3D5AB1 binds to, and inhibits ATP synthase to a greater extent than angiostatin, we next studied the effect of MAb3D5AB1 on endothelial cell tube formation. MAb3D5AB1 significantly impedes endothelial cell tube formation under conditions of acidosis. Tube formation is a measure of the angiogenic capability of endothelial cells (35). To validate these *in vitro* data, we tested the antiangiogenic potential of MAb3D5AB1 in two *in vivo* models with significantly different pHs—the low pH CAM assay and the higher pH rat corneal neovascularization assay. The reduced pH in the CAM is likely due to the function of the allantois, which is a waste reservoir for the developing chicken embryo, collecting such products as uric acid (36). MAb3D5AB1 showed significant antiangiogenic activity in the acidic environment of the CAM, validating this angiogenesis model for use in testing compounds targeting the angiostatin receptor. Although the antibody did not inhibit angiogenesis in the rat corneal neovascularization assay, this was expected given the normal tissue pH of the cornea and our *in vitro* results indicating efficacy only at low pH_e. Importantly, our data from this model indicate that MAb3D5AB1 would most likely not inhibit nonpathologic angiogenesis, such as in wound healing, occurring at the normal physiologic pH.

Since Folkman proposed in 1971 that targeting tumor vasculature might effectively halt tumor growth, the field of antiangiogenesis has progressed to include several potential antiangiogenic therapies for cancer. In preliminary phase II trials, recombinant human angiostatin combined with standard chemotherapy showed a partial response in 39% and achieved stable disease in 39% of 23 patients with non–small cell lung cancer (3).

MAb3D5AB1 can be studied for further antiangiogenic characteristics *in vitro* and *in vivo* and could be used to prevent tumor angiogenesis. Advantages of mAb therapy include high specificity, binding affinity, and limited side effect profiles. In addition, antibodies have a longer half-life in serum relative to angiostatin, and our data show that MAb3D5AB1 has similar effects to angiostatin *in vitro* and *in vivo* at considerably lower molar doses.

Acknowledgments

Received 3/23/2006; revised 2/13/2007; accepted 3/2/2007.

Grant support: Grants CA-86344 (S.L. Chi, M.L. Wahl, D.J. Kenan, C.E. Johnson, and S.V. Pizzo) and P01-CA56690 (M.L. Wahl) and Medical Scientist Training Program grant T32-GM07171 (Y.M. Mowery).

The costs of publication of this article were defrayed in part by the payment of page charges. This article must therefore be hereby marked *advertisement* in accordance with 18 U.S.C. Section 1734 solely to indicate this fact.

We thank Steven R. Conlon, Marie L. Thomas, and Thomas Venetta.

References

1. Griffioen AW, Molema G. Angiogenesis: potentials for pharmacologic intervention in the treatment of cancer, cardiovascular diseases, and chronic inflammation. Pharmacol Rev 2000;52:237–68.
2. Jain RK. Antiangiogenic therapy for cancer: current and emerging concepts. Oncology (Huntingt) 2005;19:7–16.
3. Lenz HJ. Antiangiogenic agents in cancer therapy. Oncology (Huntingt) 2005;19:17–25.
4. Cao Y, Xue L. Angiostatin. Semin Thromb Hemost 2004;30:83–93.
5. Soff GA. Angiostatin and angiostatin-related proteins. Cancer Metastasis Rev 2000;19:97–107.
6. Moser TL, Kenan DJ, Ashley TA, et al. Endothelial cell surface F1-0 ATP synthase is active in ATP synthesis and is inhibited by angiostatin. Proc Natl Acad Sci U S A 2001;98:6656–61.
7. Moser TL, Stack MS, Asplin I, et al. Angiostatin binds ATP synthase on the surface of human endothelial cells. Proc Natl Acad Sci U S A 1999;96:2811–6.
8. Wahl ML, Kenan DJ, Gonzalez-Gronow M, Pizzo SV. Angiostatin's molecular mechanism: aspects of specificity and regulation elucidated. J Cell Biochem 2005;96:242–61.
9. Apoptosis and cell proliferation. Roche Molecular Biochemicals. 2nd ed. Mannheim (Germany): Boehringer Mannheim GmbH; 1998.
10. Arechaga I, Jones PC. Quick guide: ATP synthase. Curr Biol 2001;11:R117.
11. Arakaki N, Nagao T, Niki R, et al. Possible role of cell surface H^+ −ATP synthase in the extracellular ATP synthesis and proliferation of human umbilical vein endothelial cells. Mol Cancer Res 2003;1:931–9.
12. Chi SL, Pizzo SV. Angiostatin is directly cytotoxic to tumor cells at low extracellular pH: a mechanism dependent on cell surface-associated ATP synthase. Cancer Res 2006;66:875–82.
13. Das B, Mondragon MO, Sadeghian M, Hatcher VB, Norin AJ. A novel ligand in lymphocyte-mediated cytotoxicity: expression of the β subunit of H^+ transporting ATP synthase on the surface of tumor cell lines. J Exp Med 1994;180:273–81.
14. Capaldi RA, Aggeler R. Mechanism of the F(1)F(0)-type ATP synthase, a biological rotary motor. Trends Biochem Sci 2002;27:154–60.
15. Moser TL, Stack MS, Wahl ML, Pizzo SV. The mechanism of action of angiostatin: can you teach an old dog new tricks? Thromb Haemost 2002;87:394–401.
16. Alkan SS. Monoclonal antibodies: the story of a discovery that revolutionized science and medicine. Nat Rev Immunol 2004;4:153–6.
17. Wahl ML, Grant DS. Effects of microenvironmental extracellular pH and extracellular matrix proteins on angiostatin's activity and on intracellular pH. Gen Pharmacol 2002;35:277–85.
18. Wahl ML, Owen CS, Grant DS. Angiostatin induces intracellular acidosis and anoikis in endothelial cells at a tumor-like low pH. Endothelium 2002;9:205–16.
19. Ferrara N, Hillan KJ, Gerber HP, Novotny W. Discovery and development of bevacizumab, an anti-VEGF antibody for treating cancer. Nat Rev Drug Discov 2004;3:391–400.
20. Aggeler R, Chicas-Cruz K, Cai SX, Keana JF, Capaldi RA. Introduction of reactive cysteine residues in the ε subunit of *Escherichia coli* F1 ATPase, modification of these sites with tetrafluorophenyl azide-maleimides, and examination of changes in the binding of the ε subunit when different nucleotides are in catalytic sites. Biochemistry 1992;31:2956–61.
21. Marusich MF. Efficient hybridoma production using previously frozen splenocytes. J Immunol Methods 1988;114:155–9.
22. Grant DS, Kinsella JL, Kibbey MC, et al. Matrigel induces thymosin b4 gene in differentiating endothelial cells. J Cell Sci 1995;108:3685–94.
23. Burwick NR, Wahl ML, Fang J, et al. An Inhibitor of the F1 subunit of ATP synthase (IF1) modulates the activity of angiostatin on the endothelial cell surface. J Biol Chem 2005;280:1740–5.
24. Zheng J, Ramirez VD. Piceatannol, a stilbene phytochemical, inhibits mitochondrial F0F1-ATPase activity by targeting the F1 complex. Biochem Biophys Res Commun 1999;261:499–503.
25. Owen CS. Comparison of spectrum-shifting intracellular pH probes 5′(and 6′)-carboxy-10-dimethylamino-3-hydroxyspiro[7H-benzo[c]xanthene-7, 1′(3′H)-isobenzofuran]-3′-one and 2′,7′-biscarboxyethyl-5(and 6)-carboxyfluorescein. Anal Biochem 1992;204:65–71.
26. Wahl ML, Pooler PM, Briand P, Leeper DB, Owen CS. Intracellular pH regulation in a nonmalignant and a

derived malignant human breast cell line. J Cell Physiol 2000;183:373–80.
27. Grynkiewicz G, Poenie M, Tsien RY. A new generation of Ca^{2+} indicators with greatly improved fluorescence properties. J Biol Chem 1985;260:3440–50.
28. Popov E, Gavrilov I, Pozin E, Gabbasov Z. Multiwavelength method for measuring concentration of free cytosolic calcium using the fluorescent probe Indo-1. Arch Biochem Biophys 1988;261:91–6.
29. White RR, Shan S, Rusconi CP, et al. Inhibition of rat corneal angiogenesis by a nuclease-specific RNA aptamer specific for angiopoietin-2. Proc Natl Acad Sci U S A 2001;100:5028–33.
30. Gho YS, Kleinman HK, Sosne G. Angiogenic activity of human soluble intercellular adhesion molecule-1. Cancer Res 1999;59:5128–32.
31. DeMoraes ED, Fogler WE, Grant DS, et al. Recombinant human angiostatin (rhA): A Phase I clinical trial assessing safety pharmacokinetics and pharmacodynamics [abstract #10]. Am Soc Clin Oncol 2001;20:3a.
32. Boyer PD. The ATP synthase—a splendid molecular machine. Annu Rev Biochem 1997;66:717–49.
33. Pedersen PL, Amzel LM. ATP synthases. Structure, reaction center, mechanism, and regulation of one of nature's most unique machines. J Biol Chem 1993;268:9937–40.
34. Shin YK, Yoo BC, Chang HJ, et al. Down-regulation of mitochondrial F1F0-ATP synthase in human colon cancer cells with induced 5-fluorouracil resistance. Cancer Res 2005;65:3162–70.
35. Nehls V, Drenckhahn D. A novel, microcarrier-based *in vitro* assay for rapid and reliable quantification of three-dimensional cell migration and angiogenesis. Microvasc Res 1995;50:311–22.
36. Ribatti D, Nico B, Vacca A, Roncali L, Burri PH, Djonov V. Chorioallantoic membrane capillary bed: a useful target for studying angiogenesis and anti-angiogenesis *in vivo*. Anat Rec 2001;264:317–24.